decrease the positive charge at the carbocation active center and favor free ion formation. In contrast, the chloro substituent is electron withdrawing, which would increase the positive charge at the growing carbocation center and favor the formation of solvated ion pairs. If these resonance effects occur to a significant extent, then the polymerization reaction of the *p*-chloro monomer could be much more sensitive to the environment of the carbocation active center than that of the *p*-fluoro monomer.

The values of syndiotactic and isotactic sequence lengths, as calculated from the equations above, for the fluoro-substituted series of polymers obtained in mixtures of methylene chloride and hexane or toluene are collected in Table VI. It is again clearly seen that the isotactic configuration is very difficult to form, and the average isotactic sequence length is only one for all of the polymers; that is, no units longer than diads were formed and only very few of those. The syndiotactic sequence length shows a very slight solvent effect, becoming longer with increasing solvent polarity.

Experimental Section

All polymerization reactions were carried out at −78 °C under an atmosphere of dry argon with reagents purified and dried by techniques as previously reported.[1]

Proton NMR spectra for all the polymers obtained in mixtures of methylene chloride and hexane were obtained on 10% (w/v) solutions of the polymers in *o*-dichlorobenzene at 100 °C with *p*-dioxane as the internal standard. Spectra for all the polymers obtained in mixtures of methylene chloride and toluene were obtained on 10% (w/v) solutions of the polymers in toluene-d_8 at 100 °C with *p*-dioxane as the internal standard. Triad tacticities were determined from the relative areas of the three α-methyl proton resonances.

Acknowledgment. The high-field NMR experiments were performed at the NMR Facility for Biomolecular Research located at the F. Bitter National Magnet Laboratory, M.I.T., and at the NMR Facility at the University of Massachusetts at Amherst. We are grateful to the National Science Foundation for the support of this work under Grant No. DMR 80-22273.

References and Notes

(1) Lenz, R. W.; Faullimmel, J. G.; Jonte, J. M. In "Initiation of Polymerization", Bailey, F. E., Jr., Ed.; American Chemical Society: Washington, DC, 1983; p 103.
(2) Lenz, R. W.; Sutherland, J. E.; Westfelt, L. C. *Makromol. Chem.* **1976**, *177*, 653.
(3) Lenz, R. W.; Westfelt, L. C. *J. Polym. Sci., Polym. Chem. Ed.* **1976**, *14*, 2147.
(4) "CRC Handbook of Chemistry and Physics", 56th ed.; CRC Press: Boca Raton, FL, 1984.
(5) Ramey, K. C.; Statton, G. L.; Jankowski, W. C. *J. Polym. Sci., Part B* **1969**, *7*, 693.
(6) Lenz, R. W.; Regel, W.; Westfelt, L. C. *Makromol. Chem.* **1975**, *176*, 781.
(7) Kunitake, T.; Aso, C. *J. Polym. Sci., Part A-1* **1970**, *8*, 665.
(8) Szwarc, M. *Makromol. Chem.* **1965**, *89*, 44.
(9) Braun, D.; Heufer, G.; Johnson, U.; Kolbe, K. *Ber. Bunsen-Ges. Phys. Chem.* **1964**, *68*, 959.
(10) Flory, P. J. "Principles of Polymer Chemistry"; Cornell University Press: Ithaca, NY, 1953; p 553.
(11) Higashimura, T.; Kishiro, O. *Polym. J. (Tokyo)* **1977**, *9*, 87.
(12) Lenz, R. W.; Jonte, J. M.; Gula, D. J. *Polym. Prepr. (Am. Chem. Soc., Div. Polym. Chem.)* **1985**, *26* (1).
(13) Ohsumi, Y.; Higashimura, T.; Okamura, S. *J. Polym. Sci., Part A-1* **1966**, *4*, 923.
(14) Sawamoto, M.; Masuda, T.; Higashimura, T. *Makromol. Chem.* **1976**, *177*, 2995.
(15) Imanishi, Y.; Higashimura, T.; Okamura, S. *Kobunshi Kagaku* **1960**, *17*, 236.
(16) Coleman, B. D.; Fox, T. G. *J. Polym. Sci., Part A* **1963**, *1*, 3183.
(17) Bovey, F. A. "Polymer Conformation and Configuration"; Academic Press: New York, 1969; p 41.
(18) Brown, H. C.; Okamoto, Y. *J. Am. Chem. Soc.* **1957**, *79*, 1913.

Morphology of Poly(ethylene terephthalate) Fibers As Studied by Multiple-Pulse ^{1}H NMR

John R. Havens† and David L. VanderHart*

Polymers Division, National Bureau of Standards, Gaithersburg, Maryland 20899.
Received August 20, 1984

ABSTRACT: Drawn poly(ethylene terephthalate) (PET) fibers annealed under various conditions are investigated by proton spin diffusion as detected through nuclear magnetic resonance. The primary objective is to study morphology on the 1–50-nm scale, the smaller dimensions of which have proved difficult to characterize for PET by conventional techniques. The spin diffusion experiment is comprised of three periods: generation of a magnetization gradient among different domains, relaxation of the gradient by diffusion for a variable time, and separate detection of the magnetization corresponding to each domain. The use of a multiple-pulse sequence permits spin diffusion to be confined to the second period, resulting in enhanced resolution among the domains. This procedure allows the magnetization decay observed during the detection period to be decomposed into three components, which are assigned to mobile noncrystalline, constrained noncrystalline, and crystalline domains. Rates of polarization redistribution among these three components are studied as a function of the diffusion time. Computer modeling is carried out in order to relate these measurements to the spatial arrangement and size of the three components. The results quantify the increase in crystallinity and in crystallite size upon annealing. Information pertaining to the structure of the noncrystalline region, the importance of noncrystalline chain orientation, and the relative surface areas of the crystallites is also presented.

Introduction

A. PET Morphology. Much of the usefulness of polymeric materials derives from the ability to modify their macroscopic properties by processing. To design the optimum treatment for a particular application requires a knowledge of chain structure on the 1–50-nm scale, a region which can strongly influence mechanical performance. In this work we characterize the local morphology of uniaxially oriented poly(ethylene terephthalate) (PET) fibers. Such fibers have important structure in the 3–15-nm regime. Previous efforts to characterize this region have been made through a variety of measurements: small-angle and wide-angle X-ray scattering,[1-7] heat of fusion,[5,8] density,[5,6,9]

† Present address: Raychem Corp., Menlo Park, CA 94025.

infrared,[10-15] nuclear magnetic resonance (NMR),[16-19] and optical birefringence.[16,18] Interpretation of the results has proved difficult, however, because many of these techniques give information which either is localized within a repeat unit or involves an extrapolation to the local level from an average macroscopic measurement. Another, more direct means of characterization is desirable. In this paper we assess the use of some recently developed NMR techniques to investigate the morphology of PET samples with different processing histories. Areas of particular interest include determination of percent crystallinity, validity of a two-phase (crystalline/amorphous) model, size and spatial arrangement of the domains, and structure of the noncrystalline material. We will also explore the measurement of crystallite surface area through spin diffusion behavior.

This research is part of a joint effort with Firestone Tire and Rubber Co. to examine the morphology of drawn and annealed PET fibers. Further details concerning sample preparation, physical properties, and morphological analysis by DSC and X-ray diffraction will be published separately.[20]

B. Spin Diffusion Experiment. For many heterogeneous solid samples NMR can be used to study domain sizes by monitoring spin diffusion. Common synthetic polymers, with their abundance of hydrogen, are candidates for such ^1H NMR measurements. The secular Hamiltonian describing the many-body proton–proton dipolar couplings includes a spin-exchange term. This term forms the basis for understanding magnetization transport in inhomogeneously relaxing spin systems. Spin diffusion is the name given to this transport process. The spin diffusion experiments described herein are analogous to heat conduction experiments in the presence of a temperature gradient where magnetization and temperature are the parallel quantities.

The importance of spin diffusion in interpreting magnetic resonance relaxation was recognized in the 1940s.[21] More recently, efforts to determine domain sizes in solid polymers have been made by following ^1H spin diffusion behavior. Most of this work has been based upon the Goldman–Shen experiment.[22] Polyethylene,[23,24] polyamide blends,[24] and polyurethanes[25] all have been investigated by the original Goldman–Shen sequence, which exploits a difference in T_2's to generate the magnetization gradient between domains and which records the free induction decay (FID) during the detection period. For various spin diffusion times polarization in each domain is then quantified by resolving the fast and slow contributions to the FID. Several modifications of this sequence also have been developed. In their study of PET films, Cheung et al.[26] used a difference in ^1H $T_{1\rho}$'s to generate the gradient and detected the signal during a dipolar-narrowed Carr–Purcell sequence,[27] which effectively quenches spin diffusion among the protons. Packer et al.[28] have used a $T_{1\rho}$ preparation period with detection of the free induction decay following an optional second selection period also based on ^1H spin locking. In each of these experiments, the magnetization decay during the detection period is decomposed into two or three components, the relative amplitudes of which are then correlated with the variable spin diffusion time in the laboratory frame. The rate of disappearance of the original magnetization gradient can be related to domain sizes by making a reasonable estimate of the diffusion coefficient.

Each of the spin-diffusion experiments referred to above has disadvantages if applied to PET fibers. The Goldman–Shen experiment is not appropriate for the examination of PET fibers below T_g since the noncrystalline and crystalline T_2's are comparable. Moreover, if one attempts to go above T_g for an oriented PET fiber sample in order to provide better contrast between crystalline and noncrystalline T_2's, the fibers change irreversibly. On the other hand, if one prepares magnetization gradients based on different intrinsic $T_{1\rho}$ behavior in different regions, then a certain amount of confusion results from the fact that spin diffusion proceeds even in the presence of a strong, resonant radio-frequency field, albeit the corresponding diffusion constant is only half that characterizing spin diffusion in the laboratory frame.[29] For example, a $T_{1\rho}$ preparation period of 1 ms would result in significant spin diffusion over a distance of 1 nm, thus blurring structural features at this level. Although this fuzziness can be accounted for to some extent in the mathematics of modeling the diffusion behavior, the ability to generate sharp gradients experimentally reduces both the complexity of the mathematical analysis and the ambiguity of the morphological models.

Our approach has been to use a multiple-pulse radio-frequency sequence[30,31] during the preparation period. This accomplishes two purposes. First, magnetization gradients are created by different relaxation rates of the various domains in the sample. Relaxation under multiple-pulse schemes is related to the spectral density of molecular motion in the mid-kilohertz regime.[31-33] In this respect the magnetization behavior is similar to that in the ^1H $T_{1\rho}$ experiment. The rigid crystalline regions of the sample relax slowly because the molecular motion is not centered at mid-kilohertz frequencies; moreover, the amplitude of motion is limited. The more mobile noncrystalline domains relax relatively quickly. (NMR measurements of motional rates and amplitudes in PET have been published.[34,35]) For some PET samples the time constants characterizing these exponential decays (T_{1xz}'s) differ by 2 orders of magnitude, as will be shown below. The second purpose in using multiple-pulse cycles during the preparation (and detection) period is to slow spin diffusion. Coherent averaging theory[30,31] demonstrates that the multiple-pulse schemes ideally result in elimination of the dipolar couplings among protons, which are necessary for spin diffusion to occur. In practice, the ^1H dipolar line width of crystalline polymers can be reduced by 2 orders of magnitude[36,37] using this method. Spin diffusion is then effectively quenched, and the magnetization gradients generated by mobility differences among the domains maintain their sharpness until the diffusion period in the laboratory frame begins. The suppression of spin diffusion during both preparation and detection also carries with it the advantage that heterogeneity of molecular motion in the noncrystalline regions may be identified and the corresponding domain sizes determined, even though domain sizes may be very small.

The pulse sequence we have chosen for the diffusion measurements is shown in Figure 1. The multiple-pulse scheme used in both preparation and detection periods is designated MREV-8[38,39] and may be represented as follows:

$$\tau\text{-}P_x\text{-}\tau\text{-}P_y\text{-}2\tau\text{-}P_{-y}\text{-}\tau\text{-}P_{-x}\text{-}2\tau\text{-}P_{-x}\text{-}\tau\text{-}P_y\text{-}2\tau\text{-}P_{-y}\text{-}\tau\text{-}P_x\text{-}\tau$$

where P_i denotes a 90° pulse about the ith axis in the rotating frame and where τ and 2τ signify pulse separations. This sequence is diagrammed in Figure 2. Vega and Vaughan[32] have studied the relaxation behavior for this eight-pulse sequence in the toggling frame (the interaction frame of reference defined by the radio-frequency pulses). Spin–lattice relaxation along the (101) direction in the toggling frame, normally one of the principal axes of relaxation, is characterized by the time constant T_{1xz}.

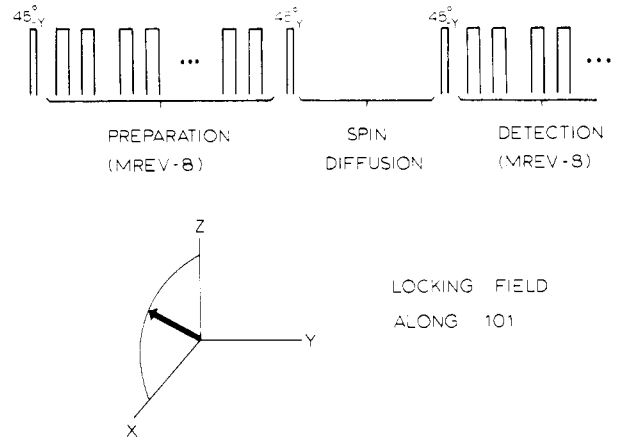

Figure 1. Pulse sequence for measuring spin diffusion rates in PET samples. Multiple pulse is performed during both preparation and detection periods. The coordinate system represents the toggling frame of reference, in which a resonance offset generates an effective spin-locking field along the (101) direction.

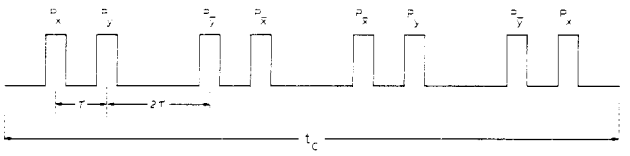

Figure 2. Representation of the MREV-8 multiple-pulse sequence. All pulses are 90°. For average Hamiltonian theory to apply, the cycle time t_c must be much less than $\|H_d\|^{-1}$, where $\|H_d\|$ is the magnitude of the dipolar Hamiltonian.

If the relaxation measurement is performed with spin-locking and if the cycle time is sufficiently short so that average Hamiltonian theory applies, T_{1xz} obeys the following equations:[32,33]

$$1/T_{1xz} = 2\Delta M_2\tau^2/9\tau_c, \qquad \text{for } \tau_c \gg \tau$$

$$1/T_{1xz} = 2\Delta M_2\tau_c/3, \qquad \text{for } \tau_c \ll \tau$$

Here ΔM_2 represents the change in the second moment due to motional narrowing, τ is the time characterizing the minimum pulse spacing in the multiple-pulse sequence, and τ_c is the correlation time of molecular motion. Through this analysis motional differences (both amplitude and frequency) among crystalline and noncrystalline domains in PET can be seen to result in different observed T_{1xz}'s. For further details concerning the specific assumptions involved in the theory of relaxation under MREV-8, the reader is referred to the work of Vega et al.[32,33]

To measure the T_{1xz}'s accurately, the magnetization must be kept along the (101) direction of the toggling frame and must not be allowed to wander in the orthogonal plane (in which relaxation is faster). We typically accomplished this spin-locking by applying the radiofrequency 5 kHz off resonance, which results in an effective field of roughly 2.5 kHz along the (101) direction. (The zero-order average Hamiltonian for an offset term under the MREV-8 cycle is proportional to $(I_x + I_z)$.[40]) The 45° pulses identified in Figure 1 are used simply to change alignment of the net magnetization between the Z axis and the (101) direction. Detection also is performed under multiple-pulse conditions, with stroboscopic observation in the 2τ window at the end of each cycle. Ideally, then, spin diffusion is isolated to that time during which magnetization is aligned along the Z axis and is quenched during both preparation and detection periods. (We note that molecular motion characterized by a correlation time $\tau_c \approx \tau$ can reduce the effectiveness of multiple-pulse decoupling and reintroduce

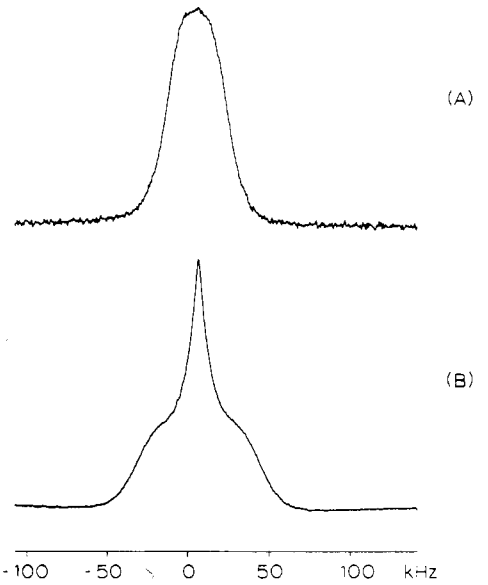

Figure 3. Proton spectra of isotropic polymers obtained from the Fourier transforms of free induction decays: (A) poly(ethylene terephthalate), sample N; (B) polyethylene, with 4 methyl groups per 1000 carbons.

spin diffusion. In such a case the conditions for average Hamiltonian theory do not apply. This does not appear to be a significant problem for the PET samples considered here, since the chemical shift spectrum recorded under multiple pulse does not display a broad resonance corresponding to domains where multiple pulse is ineffective. Instead, motional differences in crystalline and noncrystalline domains give rise to different T_{1xz}'s as predicted by the above equations, and spin diffusion appears to make only minor contributions to the behavior under multiple pulse.)

Finally, we mention a few points which make PET an attractive polymer for spin diffusion measurements. First, a wide range of PET morphologies is obtainable by varying the processing history. An amorphous material, with negligible crystallinity, can be produced by rapidly quenching the molten polymer to room temperature. Through various combinations of drawing and annealing above ~100 °C, a variety of samples of different degrees of crystallinity and molecular orientation can be obtained. Second, the ^1H T_1's (at room temperature, 200 MHz) for our PET samples under vacuum are at least 2 orders of magnitude longer than the diffusion times necessary to reach equilibrium. As a result, the total magnetization is nearly constant during the diffusion period, which facilitates modeling of its behavior. Third, the spin diffusion coefficients in different regions of the samples are more similar for PET than for many other polymers. The spin diffusion coefficient for a rigid lattice can be estimated from the second moment of the resonance obtained from an FID.[29] Polymers whose spectra have a motionally narrowed sharp resonance sitting on a much broader background have domains whose ^1H spin diffusion coefficients are domain specific; moreover, the residual line width of the narrowed component is a less definitive measure of the spin diffusion constant in that component. Such a situation exists for isotropic linear polyethylene, as shown in Figure 3. In contrast, the PET spectrum consists of only one peak, whose full width at half-maximum ranges from 28 kHz for an isotropic amorphous sample to 38 kHz for our most highly crystalline sample. A single diffusion coefficient is then sufficient to characterize all domains in the PET samples, a condition which

Table I
Poly(ethylene terephthalate) Samples

desig	history
C	control, oriented fibers, $\lambda = 5.6$
D257-0	oriented fibers, 257 °C annealed
D200-22	oriented, 200 °C annealed, free shrinkage
D200-0	oriented, 200 °C annealed, no shrinkage
Q	unoriented amorphous film, quenched
N	unoriented, quenched, 240 °C annealed

simplifies the modeling considerably.

Experimental Section

A. Samples. The PET samples used in this work were supplied by Firestone Tire and Rubber Co.[20] A list of sample designations and histories is given in Table I; the $\bar{M}_w$ of the material is approximately 45 000. Oriented fibers were obtained by extrusion from the melt, followed by elongation to a draw ratio of 5.6 by rollers operating at 110 °C. Sample D257-0 was annealed at 257 °C for 2 min under slight tension so that no shrinkage occurred. D200-0 was similarly annealed at 200 °C. D200-22 was annealed at 200 °C for 5 min without a constraint on length; final shrinkage was 22%. Sample N was an unoriented sample annealed under vacuum at 240 °C for 17 h. Each oriented sample of the PET fibers was prepared by loading fiber bundles into holes cut into a cylindrical poly(tetrafluoroethylene) holder. These holes were transverse to the cylinder axis. After cutting each fiber bundle so that it was contained within the cylinder circumference, the assembly was loaded into a 5-mm-diameter NMR tube and sealed under vacuum.

B. NMR Experiments. All measurements were performed on a Bruker CXP-200 spectrometer,[41] operating at 200 MHz for protons. Several descriptions of the design and operation of multiple-pulse spectrometers exist in the literature.[42-45] Our modifications included resistive damping of the probe circuit and use of a variable-pitch coil.[46,47] We found the most satisfactory tuning procedure for adjustment of the relative amplitudes and phases of the quadrature radio-frequency components to be that given by Burum, Linder, and Ernst.[48] Proper spectrometer tuning was verified by obtaining a scaling factor close to the theoretical value of 0.471,[36] a line width for the spectrum of calcium formate in good agreement with published results,[49] and a magnetization decay of a T_{1xz} experiment on a liquid which occurs more slowly than does the free induction decay.[32] The flatness of the receiver gain was verified by broadcasting a weak 200-MHz CW ratio-frequency signal from an antennal source a few centimeters from the coil and observing that the detected signal was constant during the application of the MREV-8 sequence.

Results

A. Proton Spin–Lattice Relaxation Measurements. A parameter which is often difficult to establish in PET fiber samples is the percent crystallinity. Since the crystallites in PET have chains with restricted mobility relative to those in noncrystalline regions,[35] an estimate of the fraction of rigid segments should correlate well with the percent crystallinity. In the absence of spin diffusion, the long T_{1xz} component represents the more rigid chains; its fraction therefore is identified with the fraction of crystalline material present in the sample. Examples of T_{1xz} decay curves are shown in Figure 4. The annealed film is expected to have more crystallinity than the control sample, and this is reflected qualitatively in a larger amount of slowly relaxing component. The pulse sequence for determining the T_{1xz} behavior is equivalent to that in Figure 1, if the preparation and spin diffusion periods are eliminated. Since magnetization equilibrium prevails at the start of the experiment, the spin temperature is uniform. This equilibrium situation also should exist for the pulse sequence in Figure 1 when the diffusion time is sufficiently long that the magnetization gradient is erased.

Two features of the decay curves in Figure 4 deserve additional comment: the oscillation which occurs during

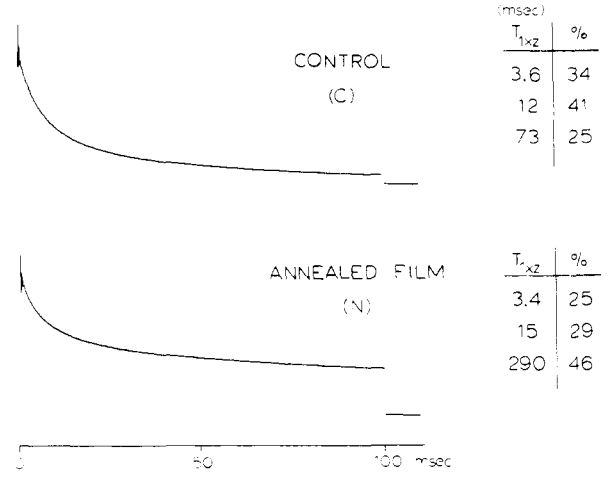

Figure 4. Measurement of T_{1xz}'s under equilibrium conditions. The pulse sequence is equivalent to that of Figure 1, with preparation and diffusion periods absent. The tables at the right indicate the decomposition of the decays into a sum of three exponentials. Base line values, corresponding to zero net magnetization, are given at the end of each decay.

the first few milliseconds and the base line at the end of the decay which represents a zero magnetization level. The oscillation arises from magnetization which is orthogonal to the spin-locking field direction in the toggling frame ((101), for a sufficiently large resonance offset). The oscillations occur at the scaled chemical shift frequencies; these oscillations complicate treatment of the data since they are present for the first ~30 points of the decay. We minimized the amplitude of the oscillation by changing the length of the "45°$_{-y}$" initial pulse and found this procedure to be preferable to the adding and subtracting of decays with different prepulses, as suggested by Vega and Vaughan.[32] More recently (after results for the PET samples had been modeled), we have succeeded in eliminating the oscillation completely by using a composite pulse[50] to rotate the magnetization from the (001) direction to (101). The composite pulse permits a canceling of the phase transients which cause deviation of the magnetization from the XZ plane during a single $-Y$ prepulse. Comparison of the results obtained by decomposition of decays with and without oscillations into a sum of exponentials indicates that the presence of the oscillation does not significantly distort the quantitative fit for the PET samples.

The second point with respect to Figure 4 concerns determination of the base line for the T_{1xz} decay. It is important to obtain an accurate estimate of this level since both the value of the long T_{1xz} and the percentage of material contributing to the long component are dependent upon the final base line chosen. After approximately 100 ms of decay under multiple pulse, the magnetization is saturated by applying ~100 successive 90° pulses, separated from each other by 100 μs and characterized by the same phase. The multiple-pulse sequence then is switched on again, and the signal is digitized at the end of each cycle. In this fashion the base line is established under the same conditions as the T_{1xz} decay. The flatness of the level also verifies the stability of the base line during MREV-8 cycles.

Decays such as those presented in Figure 4 are theoretically a sum of exponentials,[32,33] each with a separate time constant and amplitude. This distribution arises from the range of molecular motions present in a heterogeneous sample such as PET, along with possible orientation dependences. A sum of three exponentials, each with independently optimized amplitude and time constant, was selected as the simplest form which could accurately fit

Table II
Decomposition of T_{1xz} Decays

	T_{1xz}, ms			%		
sample	1	2	3	1	2	3
Q	2.6	8.9	26	35	50	15
C	3.4	12	71	33	41	26
D200-22	3.7	16	120	32	34	34
D200-0	3.0	12	95	29	37	34
D257-0	3.8	14	160	26	31	43
N	3.2	15	280	24	29	47

the data. For all samples, the agreement between calculated and observed magnetization intensities is within 1% over the time range 0–100 ms. Fitting with a sum of two exponentials results in noticeably worse agreement in the 20-ms region and in greater fluctuations in the total calculated magnetization for different spin diffusion times in the experiment in Figure 1. Certainly, a distribution of exponentials with more than three values could only improve the fit to the data. On the basis of data which we have now, a unique form of the distribution cannot be claimed. A sum of three exponentials is used because it gives a good fit to the data, is physically reasonable, and is interpretable in a straightforward fashion. The nonlinear least-squares analysis of decays for all samples is presented in Table II; values given here are averages of two independent experiments.

Other proton spin–lattice relaxation measurements, in both the rotating and laboratory frames, are given in Table III. Here $T_{1\rho}^{\Theta}$ refers to the relaxation time for magnetization spin-locked along a radio-frequency field which makes an angle Θ with the static magnetic field direction. Therefore, $T_{1\rho}^{90}$ indicates the conventional spin–lattice relaxation time measured on resonance in the rotating frame. $T_{1\rho}^{54.7}$ refers to spin–lattice relaxation detected under Lee–Goldburg conditions,[51] so that spin diffusion is slowed. By comparing the data in Tables II and III, it is clear that for the long time constants in all samples $T_{1\rho}^{90} < T_{1\rho}^{54.7} < T_{1xz}$. We would like to suggest that this trend results in large part from progressive improvement in the quenching of spin diffusion. The $T_{1\rho}^{90}$ experiment involves a reduction of the diffusion rate in the laboratory frame by a factor of 2;[29] the $T_{1\rho}^{54.7}$ measurement should completely eliminate diffusion but does not since the magic-angle condition cannot be satisfied simultaneously for all protons; and the T_{1xz} does the best job. In comparing values of the time constants, one must account for their different dependences on radio-frequency field strength, second moments, and correlation times. Published formulas[31] allow this to be done for the $T_{1\rho}^{\Theta}$'s, and after analysis it is clear that spin diffusion is quenched more effectively in the $T_{1\rho}^{54.7}$ case than in the $T_{1\rho}^{90}$. The formula is less clear in the T_{1xz} case. Evidence that the multiple-pulse sequence does, in fact, quench spin diffusion most effectively comes from the observation that only two components are sufficient to fit the $T_{1\rho}^{54.7}$ decays. The two

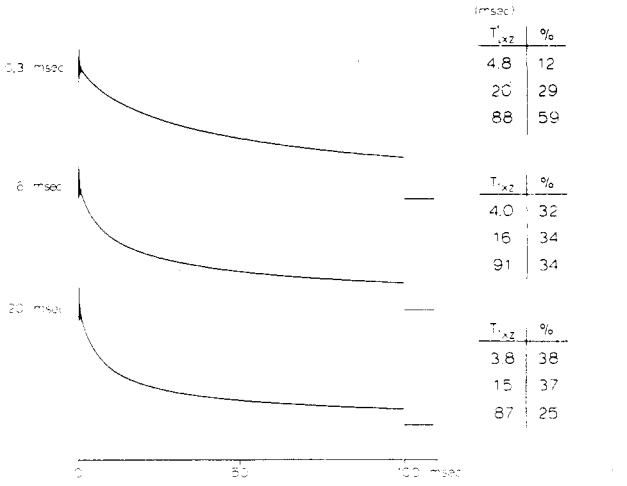

Figure 5. Representative spin diffusion measurement for sample C. The pulse sequence used is that given in Figure 1, with a 24-ms preparation period. The diffusion times in the laboratory frame are given at the left.

fastest T_{1xz} contributions are blurred by spin diffusion into one average component for both the $T_{1\rho}$ and $T_{1\rho}^{54.7}$ measurements.

B. Spin Diffusion Measurements. Magnetization decays for sample C are shown in Figure 5 for three times during which spin diffusion in the laboratory frame was permitted. The pulse sequence is that given in Figure 1. The preparation period under MREV-8 was 24 ms in length, and the applied radiofrequency was 5 kHz above resonance. As seen in Figure 5, for short diffusion times a large fraction of the magnetization exists in rigid regions characterized by the long T_{1xz}. Magnetization in the mobile regions is depleted during the preparation period. Longer diffusion times result in more magnetization being transferred to the short T_{1xz} components. Only a redistribution of polarization is involved; the total magnetization remains constant over the time required for spin diffusion to equilibrate the domain temperatures. This is true both for the experimental data and for the calculated fit based on the sum of three exponentials.

Complete spin diffusion data for sample N are presented in Table IV. Similar data were recorded for the remaining samples. An important observation is that for diffusion times on the order of 100 ms the decomposition of the decay agrees with the equilibrium decomposition given in Table II. This behavior confirms that the fast parts of the decay are intrinsic properties of the sample and do not reflect macroscopic regions (e.g., near the ends of the sample coil) where the multiple-pulse sequence could be less effective. If the latter possibility were true, the magnetization which would decay quickly because of instrumental problems could not be replenished in 100 ms by spin diffusion from regions which are separated by macroscopic distances. It could be restored only through

Table III
Proton Spin-Lattice Relaxation Times for PET Samples

	rotating frame								
	$T_{1\rho}^{90}$,[a] ms				$T_{1\rho}^{54.7}$,[b] ms				lab frame
sample	1	2	% 1	% 2	1	2	% 1	% 2	T_1, s
Q	5.4		100	0	5.3	17	56	44	6.8
C	4.5	15	40	60	6.0	43	54	46	6.5
D200-22	4.7	21	44	56	6.3	62	48	52	8.5
D200-0	5.4	21	48	52	7.1	66	52	48	8.1
D257-0	7.0	40	51	49	5.8	80	44	56	9.5
N	6.1	39	46	54	7.3	128	47	53	11.5

[a] Radio-frequency field strength of 65 kHz. [b] Radio-frequency field strength of 80 kHz.

Table IV
Spin Diffusion Measurements for Sample N

		T_{1xz}, ms			%		
diff time, ms	$M(0)$	1	2	3	1	2	3
0.3	20714	3.9	23	357	6	14	80
1	20732	3.4	19	347	8	15	77
3	20665	3.7	18	345	12	16	72
6	20885	3.3	16	339	15	20	65
10	20728	3.7	17	340	18	21	61
20	20318	4.3	17	340	21	24	55
35	20934	3.2	15	290	23	27	50
60	20615	3.7	16	298	25	27	48
100	20628	3.7	16	299	25	28	47
150	20887	3.3	14	276	24	29	47
200	21106	3.2	14	271	24	29	47
∞[a]		3.2	15	279	24	29	47

[a] Equilibrium.

the T_1 process, which for these PET samples occurs on the order of 10 s.

The trend seen in Table IV of generally longer T_{1xz}'s determined for short diffusion times is observed throughout the sample set. The most reasonable explanation for this behavior recognizes that the decay curves represent a distribution of exponentials, as would be expected from the known existence of motional heterogeneities in semicrystalline polymers. Our fitting procedure demonstrates that the range of exponentials can be approximated well by considering a trimodal distribution. The three T_{1xz} values reported for each decay then represent the centers of the distributions but do not imply that the relaxation rate within each of the three domains is entirely homogeneous. With such a trimodal distribution the preparation period discriminates against the shorter time constants in each domain, causing the centers of the distributions to be shifted to longer values. Short spin diffusion times are insufficient to reestablish the equilibrium values of the time constants. These considerations are particularly important for the noncrystalline material, since the preparation of 24 ms can distort the distribution of the short time constants more effectively than it can distort that of the long. To the extent that some variation in mobilities is allowed within each region, it is also reasonable that the more mobile crystalline material is in closer proximity to the noncrystalline regions and therefore would experience preferential depletion at short spin diffusion times. Using similar arguments, we suggest that the more rigid chains in the two noncrystalline regions would be the first to receive polarization via spin diffusion immediately following the preparation period. These effects would result in longer time constants being observed at short spin diffusion times.

C. Modeling of Spin Diffusion. To obtain information concerning the size and spatial arrangement of domains with different T_{1xz}'s, it is necessary to model the rates of equilibration exemplified by Table IV. The equation which describes the spin diffusion process and the continually changing magnetization gradient is given as follows:

$$\partial M(\vec{r},t)/\partial t = D(\vec{r})\nabla^2 M + R(\vec{r})(M_{eq} - M)$$

where M represents the magnetization concentration and is a functon of the spatial coordinates $\vec{r}$ and the time t, M_{eq} is the equilibrium magnetization concentration, D is the diffusion coefficient, and R is a parameter characterizing the contribution of T_1 processes to $\partial M/\partial t$. This equation describes classical diffusion with contributions from dissipative processes accounted for by the R term; it is derived in standard texts on heat conduction.[52,53] By considering diffusion at short times in one dimension from an extended source and by neglecting the R term, another useful equation can be derived through integration by parts (vide infra):

$$\langle x^2 \rangle = (4/3)Dt$$

where $\langle x^2 \rangle$ is the mean square displacement resulting from diffusion during a time t.

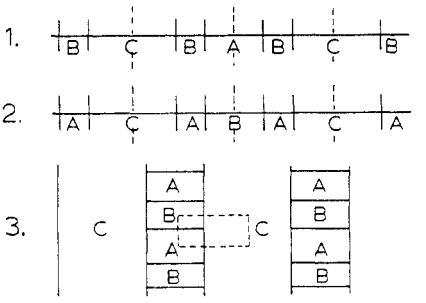

Figure 6. Three-component models used in the solution of the diffusion equation. Dashed lines indicate where boundary conditions are applied. Vertical solid lines (vertical and horizontal in model 3) specify interface positions. A represents the mobile noncrystalline domains, B the constrained noncrystalline domains, and C the crystalline domains.

With these diffusion equations we are now ready to consider specific models for PET morphology. The models are composed of three distinct phases to correspond to the three T_{1xz}'s resolved from the decays. Relative sizes of the three phases are chosen to be consistent with the equilibrium decompositions of Table II. With this information and with appropriate initial conditions (discussed later), the diffusion equation can be solved numerically. The rate of change of magnetization from the calculation then can be compared with experimental observation to determine the validity of the model. The specific models under consideration are shown in Figure 6. The mobile noncrystalline material is represented by A, the constrained noncrystalline material by B, and the rigid crystalline material by C. The regions actually modeled are those enclosed by the dashed lines. By proper choice of the boundary conditions discussed below, these regions may be reflected across the boundaries to form symmetrical repeating structures. The first two models assume planes of infinite dimension, and diffusion is restricted to the dimension perpendicular to the interface between planes. The third model is a hybrid of the first two, in that both the mobile and constrained noncrystalline regions have interfaces with the crystalline material as well as with each other. Here diffusion is permitted in two dimensions. The structure is assumed infinite in the direction normal to the plane of the figure.

1. Boundary, Interface, and Initial Conditions. We now describe formulation of the models in terms of mathematical conditions on the diffusion equation. The boundary condition $dM/dx_i = 0$ is selected for the spin diffusion problem and must be satisfied at each point along the dashed lines in Figure 6; x_i is the direction normal to these segments. Physically, this condition specifies that no net magnetization flows across the dashed lines. It also validates the solution obtained by analyzing one unit for the entire infinite structure formed by reflecting domains across the boundaries.

Continuity conditions of density and flux of magnetization also must be satisfied across all interfaces:

$$M|_{\Gamma-} = M|_{\Gamma+}$$

$$D\frac{\partial M}{\partial x_i}\bigg|_{\Gamma-} = D\frac{\partial M}{\partial x_i}\bigg|_{\Gamma+}$$

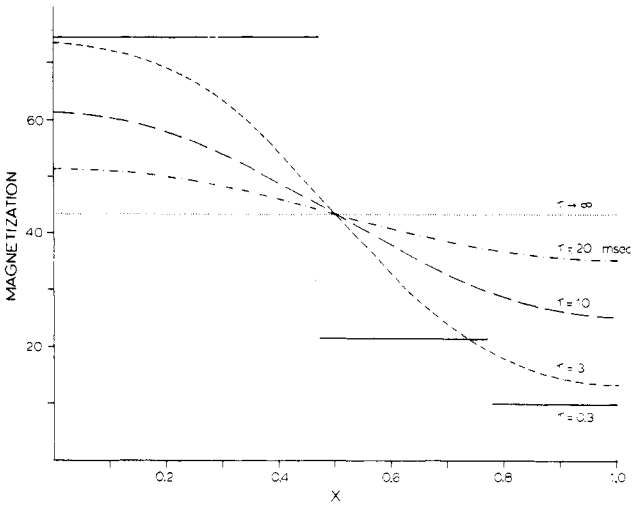

Figure 7. Diffusion profiles for sample N, calculated by numerically solving the diffusion equation in one dimension. The profiles are based on model 1 of Figure 6. The magnetization level is plotted on the ordinate. The abscissa is divided into crystalline, constrained noncrystalline, and mobile noncrystalline domains, whose sizes are indicated by the lengths of the solid horizontal lines which also represent the initial magnetization gradient (τ = 0.3 ms). Diffusion times are given on the right.

where Γ denotes an interface and the symbol $|_{\Gamma^+}$ indicates a limiting value taken from the right (above) if the interface is vertical (horizontal) and $|_{\Gamma^-}$ is the corresponding value taken from left (below). The continuity condition on magnetization is physically reasonable for all diffusion times $t > 0$. The second relation refers to flux continuity at the interfaces. This condition stipulates that the interfaces cannot act as independent sources or sinks of magnetization.

Initial conditions must also be required for a numerical solution to the diffusion equation. Knowledge of the magnetization level in each domain at an early time in the diffusion experiment is desirable. We estimate these levels by considering the decomposition of a T_{1xz} decay accumulated after a short (300 μs) period of spin diffusion. The magnetization integrals which are obtained from the decomposition must then be converted into magnetization levels by considering the relative domain sizes from Table II. Because the gradients at t = 300 μs are assumed to be perfectly sharp, calculated magnetization levels at short diffusion times ($\leq$1 ms) may be incorrect. For this reason t = 3 ms is the first diffusion time for which agreement between calculated and experimental results is used to judge the validity of the model.

The relaxation term in the diffusion equation is characterized by a rate R, which is different for each of the domains in the model. R represents the rate of recovery of magnetization due to laboratory-frame spin–lattice relaxation. For the PET samples under study all proton T_1's are at least 2 orders of magnitude longer than the time required to equilibrate spin temperatures in the three domains (cf. Table III). Therefore, all R values are small and have little effect on the solutions of the diffusion equation. For heterogeneous polymers with substantially shorter T_1's, the determination of accurate R values for the different domains is an important part of modeling the morphology by spin diffusion.

2. Solutions. With the foregoing information, one can calculate a numerical solution to the diffusion equation, with magnetization profiles given for various diffusion times. Numerical solutions were obtained through DISPL, a software package written by Leaf et al. at Argonne National Laboratory.[54] Representative results for sample N

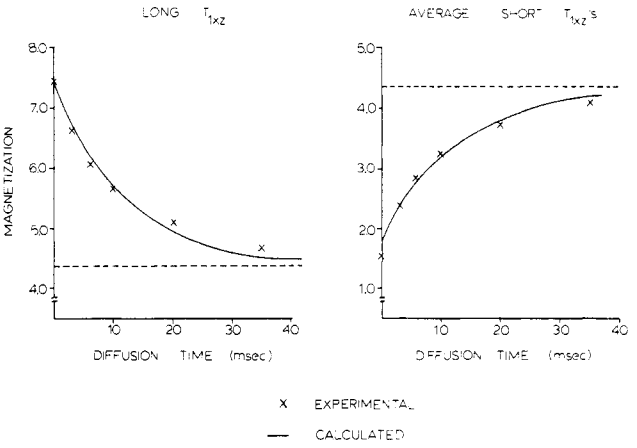

Figure 8. Comparison of calculated and observed diffusion for sample N. Calculations are based on the one-dimensional models of Figure 6. Magnetization levels are plotted on the ordinate, with the dashed lines indicating the equilibrium levels.

are shown in Figure 7. Here the magnetization level is given in arbitrary units as a function of position. The calculation is based upon the first (one dimensional) model of Figure 6. The magnetization levels at 300 μs are represented by the solid horizontal line segments in Figure 7. After longer diffusion times the gradients are attenuated, until finally a uniform magnetization density exists throughout the sample. (The intersection of the diffusion profiles at a single point is consistent with the behavior of an extended source of infinite extent.[53])

For each model under consideration, the calculated magnetization integral and average magnetization level for each domain can be compared to those from experimental observation. Agreement over the entire range of diffusion times is expected. For convenience, the single parameter which was varied to improve the fit was the diffusion coefficient D, rather than a scaling factor for the domain dimensions. From this best-fit value of D (indicated by D^*), the scaling factor for the domain dimensions was determined. The relationship between D and x dictates that an increase in D by a factor f is equivalent to scaling x by $f^{-1/2}$ at constant D.

Values of the diffusion coefficients were varied in steps of 0.5×10^{-12} cm^2/s, and those which fit the experimental data best were selected for the calculations of domain size. In order to convert this scaling factor to real dimension, the value of D appropriate to PET was estimated. By taking the diffusion coefficient of polyethylene (PE) to be 6.2×10^{-12} cm^2/s[58] and by assuming that the diffusion constant should scale as the concentration of protons to the $^1/_3$ power, a reasonable estimate of 5.0×10^{-12} cm^2/s is obtained for the diffusion coefficient of PET. For the two-dimensional model D was varied independently in both dimensions. With DISPL it is also possible to specify different D's for the various domains. While this flexibility is not required for PET, it would be necessary for any polymer which exhibits a strong contrast in T_2 behavior.

Figure 8 shows the best fit obtained between observed and calculated magnetization levels for sample N. The first model of Figure 6 was used to establish conditions on the diffusion equation. The agreement in Figure 8 suggests that the first model is a good representation of the annealed film morphology. However, the plot on the right is for the *average* of the short T_{1xz} components; the agreement for each of the individual constituents is not nearly so good, as seen in Figures 10 and 11. This indicates that the noncrystalline domain structure is not well represented by the first model. In Figures 9–11 the best fits for all

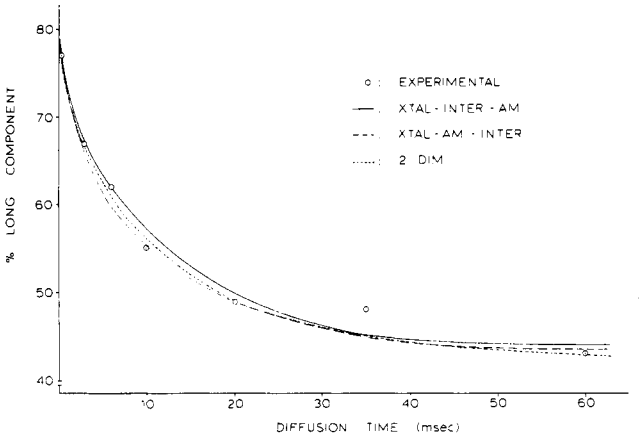

Figure 9. Plot of percentage of magnetization contributing to the long T_{1xz} as a function of diffusion time. Experimental data are for sample D257-0. The curves represent the best fits for calculated results for the three models.

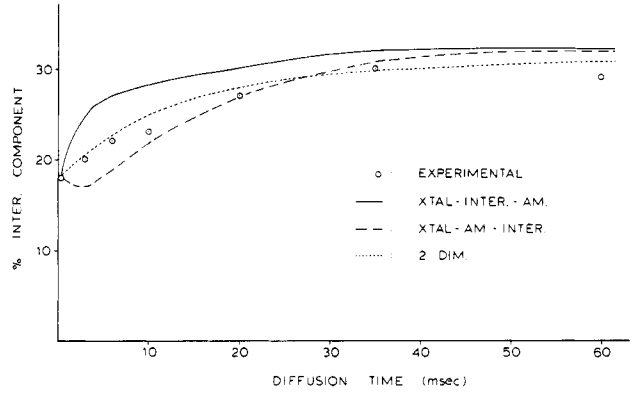

Figure 10. Plot of percentage of magnetization contributing to the intermediate T_{1xz} as a function of diffusion time. Experimental data are for sample D257-0. The curves represent results calculated from the same parameters as those used in Figure 9.

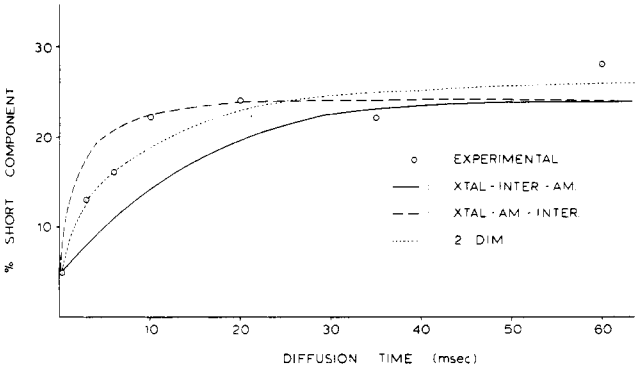

Figure 11. Plot of percentage of magnetization contributing to the short T_{1xz} as a function of diffusion time. Experimental data are for sample D257-0. The curves represent results calculated from the same parameters as those used in Figure 9.

three components are shown for each of the models. Here magnetization integrals are presented for D257-0. Similar behavior also is exhibited by the other samples. Figure 9 indicates that all these models provide equally good fits to the dependence of the amount of rigid component on diffusion time. The diffusion coefficients were optimized for this component and then held fixed. Figures 10 and 11 depict the behavior of the noncrystalline regions of the sample and allow differentiation among the models in terms of quality of fit. The worst agreement between observed and calculated recovery is obtained for the first model. The two-dimensional model provides a slightly better fit than the second, especially in the early diffusion time regime.

Table V
PET Domain Sizes for One-Dimensional Models

sample	D^*	L, nm	domain size, nm: xtal	inter	amorph	% xtal
C	16.0	11.2	2.9	2.3	3.7	26
N	8.0	15.8	7.4	2.3	3.8	47
D257-0	7.5	16.4	7.1	2.6	4.1	43
D200-22	15.0	11.6	3.9	2.0	3.8	34
D200-0	13.0	12.4	4.2	2.3	3.6	33

Table VI
PET Domain Sizes (nm) for Two-Dimensional Model

sample	xtal r	inter r	inter z	amorph r	amorph z	% xtal	long period r	long period z
C	2.9	8.3	4.4	8.3	3.6	26	11.2	8.0
N	7.4	8.4	6.2	8.4	5.0	47	15.8	11.2
D257-0	7.0	9.4	6.4	9.4	5.2	43	16.4	11.6
D200-22	4.0	7.6	4.0	7.6	4.2	34	11.6	8.2

Table VII
Percent Crystallinities

sample	NMR	DSC[a]	ρ[a]	WAXS[a]	lit. values[b]: DSC	ρ	WAXS
C	26	46	42	54		13	28[d]
N	47						
D257-0	43				48	54	39[f]
D200-22	34	42	47	65			39[f]
D200-0	33	46	50	65	47	43	41[d]

[a] Reference 20. [b] These values correspond to samples whose treatment was similar to those used in this study. [c] Reference 5. [d] Reference 55. [e] Reference 8. [f] Reference 18.

Table VIII
Long Periods (nm)

sample	L NMR	ax L SAXS[a]	transverse L SAXS[a]	lit. values[b]: ax L SAXS
C	11.2	16.1	8.7	17.5[c]
D257-0	16.4	17.9	13.6	18.4[d]
D200-22	11.6	14.1	17.0	13.2[e]
D200-0	12.4	15.5	11.1	12.2[d]

[a] Reference 20. [b] These values correspond to samples whose treatment was similar to those used in this study. [c] Reference 12. [d] Reference 5. [e] Reference 6.

Once the optimum value of the diffusion coefficient has been found for each of the models, the domain sizes can be calculated directly. This information is presented in Table V for the two one-dimensional models. Despite the observation from Figures 10 and 11 that the second model fits the experimental values considerably better than does the first, the optimum agreement for both models occurs for the same diffusion coefficient. The calculated domain sizes then are the same for the two linear models, although the spatial arrangements are different. The quantity labeled L in Table V is the structural repeat distance in the models and corresponds to twice the distance enclosed by the dashed boundary lines in Figure 6. This number is the analogue of the long period determined by small-angle X-ray scattering. In Table VI results from the two-dimensional model are shown. The letter r represents the horizontal direction in Figure 6; z represents the vertical. Diffusion coefficients were optimized independently for each of the dimensions.

We are now able to compare the crystallinity and long-period results from NMR with those from X-ray,

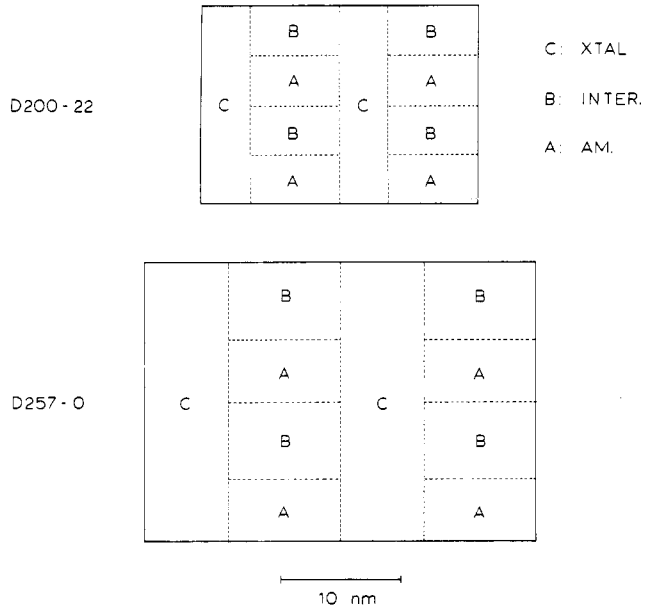

Figure 12. Representation of the morphology of two PET fibers. Results are calculated from a two-dimensional solution to the diffusion equation. Both vertical and horizontal directions are drawn to the indicated 10-nm scale. Region C has infinite dimension in the vertical direction.

DSC, and density measurements. These data are shown in Tables VII and VIII. Values obtained from the literature for similarly treated samples are also presented. The NMR crystallinities are regarded as the fractions of the long T_{1xz} component recorded in decays from equilibrium under multiple pulse. The NMR long periods apply to both the one- and two-dimensional modeling results for the repeat distance between consecutive crystalline lamellae. Finally, we present in Figure 12 schematic drawings of the morphology for two of the PET fibers, calculated from the spin diffusion results. The models are drawn to scale and represent the best fit to the experimental data for the simplified block structures which we have considered. On the basis of experiments which we will not detail here, the crystallinities as determined by NMR are considered to be accurate to within ±5%. A reasonable estimate of the uncertainty in domain sizes is ±0.6 nm.

D. Relative Crystallite Surface Areas. The interfaces between different domains in a heterogeneous polymer can influence much of its macroscopic behavior, yet the detailed nature of the interface, as well as the area it covers, is typically difficult to characterize. For the PET fibers considered here, we would like an estimate of the crystalline/noncrystalline surface area in a given volume of sample. On a relative basis such information can be extracted from the initial magnetization recovery as a function of spin diffusion time. Thus, the ratios of crystallite surface areas for different samples can be correlated with annealing treatment. Since we are interested primarily in relative surface areas of the crystallites, a two-phase, crystalline/noncrystalline model suffices. The two short T_{1xz} fractions are summed to comprise the noncrystalline component. This simplification allows exact analytical solutions to be used in dealing with the spin diffusion behavior. We first summarize our approach to the problem and follow this with a more rigorous justification of the procedure. Finally, we present the experimental observations.

1. Summary of Approach. After preparation of a magnetization gradient under multiple pulse, the higher level of polarization present in the crystallites causes magnetization to diffuse into noncrystalline regions. The amount of magnetization which flows via spin diffusion during a time t into the noncrystalline domains is designated $\Delta M^{NC}(t)$, where $\Delta M^{NC}(t) = M^{NC}(t) - M^{NC}(0)$. For short diffusion times $\Delta M^{NC}(t)$ is directly proportional to the size of the initial magnetization gradient (at time t = 0), to the surface area though which diffusion occurs, and to some function of time which characterizes the diffusion rate. We can formulate this relationship as

$$\Delta M^{NC}(t) \propto [\tilde{M}^{C}(0) - \tilde{M}^{NC}(0)]Af(t)$$

where $\tilde{M}^{C}(0)$ represents the crystallite magnetization level (total magnetization in the crystallites divided by the fraction crystallinity) at time 0, A is the total surface area of the crystallites in a given volume, and $f(t)$ represents the time dependence of noncrystalline magnetization growth. As shown in the following section, $f(t)$ is proportional to $t^{1/2}$ for sufficiently short diffusion times, but the specific functional form of $f(t)$ is not critical in determining relative surface areas. The important factor is that we consider only those diffusion times short enough so that the same $f(t)$ applies equally well for all samples—in other words, so that differences in domain sizes do not cause variations in the rates of propagation of the magnetization fronts. Thus, the diffusion times used in the analysis must be shorter than the time required for two diffusing magnetization fronts to meet in the middle of either crystalline or noncrystalline domains. If this condition is met, the crystallite surface areas of two samples can be compared, since both $\Delta M^{NC}(t)$ and $[\tilde{M}^{C}(0) - \tilde{M}^{NC}(0)]$ are experimentally measurable. Slopes of plots of $M^{NC}(t)$ vs. $t^{1/2}$ can be ratioed (after appropriate corrections) to yield the desired surface area information.

2. Justification. The crystalline/noncrystalline finite-phase system corresponds to the one-dimensional lamellar models presented in Figure 6, if the two noncrystalline regions are assumed to be indistinguishable. Crank[53] has solved the diffusion equation analytically for such a system; the following conditions describe the situation. The magnetization is present initially only in the crystalline region with a concentration C_0. This region extends from $x = 0$ to $x = h$. The magnetization diffuses at times $t > 0$ into the noncrystalline region of width $l - h$, which has an initial concentration of 0. Reflecting boundary conditions are applied at $x = 0$ and $x = l$ such that $dC/dx = 0$, where $C = C(x,t)$ is the concentration of magnetization. The profile of concentration after diffusion has occurred for time t is given as

$$C = 0.5C_0 \sum_{n=-\infty}^{\infty} \left\{ \text{erf} \frac{h + 2nl - x}{2(Dt)^{1/2}} + \text{erf} \frac{h - 2nl + x}{2(Dt)^{1/2}} \right\}$$

where erf z is the error function, defined by

$$\text{erf } z = (2/\pi^{1/2}) \int_0^z e^{-\eta^2} \, d\eta$$

The experimental observable of interest is ΔM^{NC}, which in this case is equal to $\int_h^l C \, dx$. From the above expression for C, it is clear that ΔM^{NC} is directly proportional to C_0, the initial size of the magnetization gradient. It is also readily apparent from the nature of the model that ΔM^{NC} scales directly with the amount of surface area through which diffusion occurs. Unfortunately, the time dependence of ΔM^{NC} is less easily evaluated, since it involves the integral of an infinite series of error functions.

To simplify matters somewhat, we consider the following system, whose behavior will be identical with that considered above for sufficiently short diffusion times. Just before diffusion begins (t = 0), the magnetization is dis-

tributed such that $C = C_0$ for all $x \leq 0$ and $C = 0$ for all $x > 0$. Under these conditions the solution to the diffusion equation is given by[53]

$$C(x,t) = 0.5C_0 \text{ erfc } x/2(Dt)^{1/2}$$

where the error-function complement, erfc z, is defined by

$$\text{erfc } z = 1 - \text{erf } z = (2/\pi^{1/2}) \int_z^\infty e^{-n^2} \, d\eta$$

Now the integral representing the total noncrystalline magnetization becomes more tractable:

$$\Delta M^{NC}(t) = \int_0^\infty C(x,t) \, dx = C_0(Dt/\pi)^{1/2}$$

From this result it is clear that for short diffusion times (before the magnetization fronts feel the finite sizes of the domains) the noncrystalline magnetization grows with $t^{1/2}$.

A remaining question is how long this $t^{1/2}$ dependence can be expected to apply in a system with finite domain sizes, such as the one-dimensional, crystalline/noncrystalline model. A reasonable approximation is that the $t^{1/2}$ behavior will be observed until two magnetization fronts diffusing in opposite directions meet in the center of either the crystalline or noncrystalline domains. (Unfortunately, the magnetization front is a somewhat nebulous quantity, since it becomes increasingly diffuse as time progresses. This tends to make the deviation from $t^{1/2}$ behavior a gradual one, but we feel that the meeting of fronts offers a useful guide to the point at which this deviation becomes considerable.) The front position can be defined by the root mean square displacement, $\langle x^2 \rangle^{1/2}$, which is in turn defined by

$$\langle x^2 \rangle = \int_0^\infty x^2 C \, dx / \int_0^\infty C \, dx$$

Using the above expression for C in terms of the error-function complement and again being restricted to short diffusion times, we can integrate by parts and obtain

$$\langle x^2 \rangle = (4/3)Dt$$

This result can be compared with the well-known solution for an instantaneous δ-function source, which has been used in previous spin diffusion studies:[26,28]

$$\langle x^2 \rangle = 2Dt$$

Estimates of finite domain size based on this latter formula are probably too large. Using the first formula and assuming a diffusion constant of 5.0×10^{-12} cm^2/s, we calculate that in 4 ms the magnetization front will move roughly 1.6 nm, while in 20 ms of diffusion it will move ~3.7 nm. These dimensions are approximately half those of the thinnest dimension in samples C and N (see Table VI). Therefore, we can expect that the magnetization recovery in the noncrystalline regions will be linear in $t^{1/2}$ for at least the first 4 ms with sample C and for ~20 ms with sample N. After these times the magnetization fronts should meet, and the rate of growth of ΔM^{NC} will be reduced.

3. Experimental Results. Plots of magnetization in the noncrystalline domains vs. $t^{1/2}$ are shown in Figure 13 for two PET samples. The horizontal dashed lines indicate the equilibrium level of noncrystalline magnetization. The experimental points appear to be linear with $t^{1/2}$ out to roughly 10 ms, at which point the rate of growth slows. The broadening of the magnetization fronts with increased diffusion time is probably responsible for the absence of sharp deviations from linearity after 4 and 20 ms of diffusion, as expected from the calculations in the previous section. Nevertheless, the linearity with $t^{1/2}$ for the first several milliseconds of diffusion is properly predicted and observed, as is the ultimate deviation from linearity due to finite domain size.

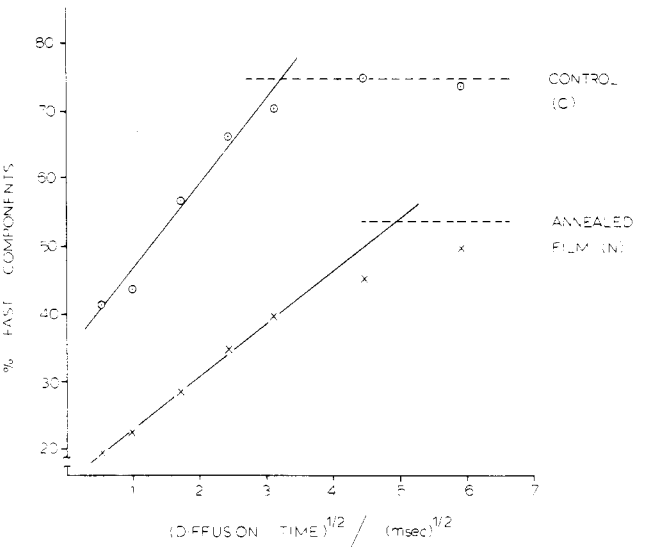

Figure 13. Plot of the percentage of magnetization contributing to the two short T_{1xz} components as a function of the square root of the diffusion time. The slopes at early times yield information concerning the relative crystallite surface areas.

Table IX
Relative Surface Areas from M vs. $t^{1/2}$ Plots

sample	measd slope	corr factor	A/A_c	model A/A_c	A/A_c[a]
C	13.7	0.59	1.0	1.0	1.0
N	7.8	0.75	0.72	0.71	0.73
D257-0	8.0	0.72	0.71	0.68	0.70
D200-22	13.3	0.56	0.92	0.97	0.97
D200-0	13.3	0.61	1.0	0.90	

[a] Slopes determined from magnetization integrals resulting from the two-dimensional calculations.

Relative crystallite surface areas can be obtained from the slopes of the linear sections of such plots. Rewriting the earlier proportionality, we have

$$\frac{M^{NC}(t) - M^{NC}(0)}{\tilde{M}^{C}(0) - \tilde{M}^{NC}(0)} = KAt^{1/2}$$

where K is a proportionality constant which is the same for all samples at short diffusion times. What has been measured experimentally and plotted along the ordinate of Figure 13 is

$$M^{NC}(t)/(\chi^{C}\tilde{M}^{C}(0) + \chi^{NC}\tilde{M}^{NC}(0))$$

where χ^C represents the mass fraction crystallinity. Therefore, the slopes obtained from Figure 13 must be multiplied by a correction factor

$$(\chi^{C}\tilde{M}^{C}(0) + \chi^{NC}\tilde{M}^{NC}(0))/(\tilde{M}^{C}(0) - \tilde{M}^{NC}(0))$$

so that the corrected slopes are directly proportional to A with K as the sample-independent proportionality constant. All parameters in this expression are determined experimentally by procedures described earlier. The correction factor accounts for different total magnetizations existing after the preparation period and for different initial gradients among the various samples.

The surface area data are compiled in Table IX. Experimental surface area ratios relative to sample C are presented, as are ratios calculated from the best fits of the

one-dimensional models. The final column consists of surface area ratios obtained by measuring slopes for magnetization integrals calculated from the two-dimensional modeling. For optimum fits of the two D^* parameters (one for each dimension), the magnetization in the noncrystalline domains was calculated for several diffusion times by numerically solving the diffusion equation and was plotted as if it were experimental data. The slopes of the calculated $\Delta M^{NC}(t)$ vs. $t^{1/2}$ curves were measured and corrected, just as they had been for the experimental data. The relative surface areas determined in this fashion should also agree well with those calculated directly from the one-dimensional model if the outlined approach to measuring relative surface areas is valid. While agreement between the surface areas derived from the experimental and calculated $\Delta M^{NC}(t)$ vs. $t^{1/2}$ curves is expected from the fact that the models (particularly the two-dimensional model) fit the data, it is gratifying that this internal consistency can be demonstrated. However, we emphasize that for short diffusion times, the relative surface area measurements do not rely on a particular model of the morphology.

Discussion

Since this work is based on the decomposition of T_{1xz} decays, it is important to understand what each component of the decays represents in terms of polymer structure. We mention first that little or none of the multicomponent character of the decays is generated by a difference in relaxation behavior beteen aromatic and aliphatic protons. Both the decomposition percentages of Table II and the recovery rates of Table IV are inconsistent with this possibility. In particular, after preparation of the magnetization gradient, up to 10 ms of diffusion is required for the two shortest T_{1xz} components to attain their equilibrium ratio. This is considerably longer than would be expected if these components were due to aromatic and aliphatic protons, which are separated only by fractions of a nanometer and therefore should equilibrate quickly. Furthermore, English[35] has analyzed rotating-frame relaxation for PET in which hydrogens on the aliphatic carbons have been replaced by deuterium and for PET with aromatic hydrogens replaced by deuterium. In this way it is possible to approximate the intrinsic relaxation behavior for aliphatic and aromatic protons. At room temperature the ^1H $T_{1\rho}$'s determined at 50 kHz are roughly the same (on the order of 10 ms) for both aromatic and aliphatic protons.[35] It is perhaps more for this reason that the T_{1xz}'s of aliphatic and aromatic protons fail to generate the multicomponent character of the decay under multiple pulse. We can then assign the T_{1xz} components to motionally distinct regions of the polymer. Some care in the assignments is necessary, however, because of the well-known fact that more efficient NMR relaxation does not necessarily imply a higher frequency of motion.[29] As mentioned earlier, relaxation rates are determined by both spectral densities and amplitudes of relevant motions. English[35] has studied motions in PET through analysis of proton line shapes and spin–lattice relaxation over a wide temperature range. He concludes that the relaxation in both rotating and laboratory frames is dominated by high-frequency motions whose amplitudes change considerably with temperature. From these results we surmise that amplitude differences are responsible in large part for the multicomponent nature of the T_{1xz} decays. Larger amplitude motions would be expected in regions with greater free volume. This picture is consistent with assigning the short T_{1xz} to a mobile noncrystalline, or "amorphous" region, the intermediate T_{1xz} to a constrained noncrystalline region, and the long T_{1xz} to a crystalline region. More concrete support for the crystalline/noncrystalline assignments comes from two observations. First, the quenched sample (Q) is characterized by short T_{1xz}'s, as indicated in Table II. Samples prepared in this fashion are thought to be amorphous in nature; they exhibit no crystallinity by X-ray diffraction. Second, annealing above T_g is known to induce crystallization in PET fibers. A clearly defined increase in the long T_{1xz} component occurs simultaneously, again shown in Table II.

With the relationship established between components of the T_{1xz} decay and domains in the samples, we offer the following comments concerning PET morphology. The percent crystallinity measurements from NMR (Table VII) agree poorly with those from DSC, density, and wide-angle X-ray scattering.[20] However, the agreement among DSC, density, and WAXS results is also poor, as is that between values reported in the literature and those measured for the samples we used. In the face of these problems, we suggest that NMR may be an attractive alternative for crystallinity measurements. The monotonic increase in crystallinity with higher annealing temperatures and longer annealing times has been reported previously for other PET sample sets[5,55,56] and is clearly indicated by the NMR data, in contrast to the DSC. Moreover, the NMR approach does not invoke the two-phase model nor does it require independent knowledge of the heat of fusion or density of the phases, as do the other techniques. Distinguishing domains on the basis of mobility, as is done with the NMR measurements, may prove more reliable than other methods applied to date.

An attractive feature of the spin diffusion measurements is that direct information concerning both noncrystalline and crystalline regions is obtained. This is particularly important for PET, where it is the structure and orientation of the noncrystalline domains which largely determine mechanical properties. One immediate consequence of the NMR analysis is that the noncrystalline material is divided into two domains which are separated from one another by a distance on the order of a few nanometers. We conclude that the two-phase crystalline–amorphous model is a poor representation of PET fiber morphology, in agreement with earlier data concerning X-ray intensities.[5] From Table II it is also clear that annealing does not preferentially crystallize either mobile or constrained noncrystalline chains. Both fractions are reduced by approximately the same amount. Therefore, a picture in which only constrained noncrystalline material is in close proximity to the crystallites and easily crystallized by annealing is not entirely accurate. Roughly the same number of mobile noncrystalline chains crystallize.

The reduction in mobile noncrystalline material upon annealing suggests that at least part of it abuts upon the crystallites. This idea is confirmed by models of the diffusion behavior. From Figure 11 it is clear that the experimental data are better fit by models in which the mobile noncrystalline regions regain magnetization at a rate higher than that expected if these regions were surrounded entirely by constrained noncrystalline chains. Similarly, Figure 10 suggests that the relatively rigid noncrystalline material does not monopolize the crystal interfaces. The best fit of the data, especially at short diffusion times, is provided by the two-dimensional model. This indicates that each of the three domain types has interfaces connecting that region to the other two. Further detail concerning spatial arrangement of the domains cannot be extracted from the modeling as it stands now. We note, however, that the above comments are consistent

with the existence of mosaic blocks in the crystallites. Fakirov et al.[8] have suggested that the grain boundaries between blocks are comprised of chains whose density is equal to that found in amorphous PET. Such chains could account for the fastest relaxing component of the noncrystalline material observed in the spin diffusion experiment. This explanation is speculative, however.

Table VIII shows that the long periods determined by NMR are in reasonable agreement with those from small-angle X-ray scattering. The agreement is roughly as good as that between the X-ray results reported here and those gathered from the literature for similar samples. From Table VI the transverse long periods (along the vertical z direction) determined by the two-dimensional model are consistently shorter than the axial long periods, in agreement with the X-ray results. This comparison is not strictly valid, however, since the NMR measurement is sensing periodicity of the two noncrystalline domains, whereas X-ray is measuring periodicity of crystalline regions transverse to the draw direction. The sensitivity to structure both parallel and perpendicular to the draw direction is a clear advantage of the X-ray method. The NMR results are dominated by periodicity in structure along the direction of the smallest dimension of the crystallites. However, the spin diffusion modeling does allow direct estimation of the size of the noncrystalline regions—something unattainable through small-angle X-ray measurements.

All results in Tables V, VI, and VIII support the increase in long period with annealing. Higher temperatures appear to be more effective in this regard than longer times, on the basis of comparing data from samples N and D257-0. This is consistent with X-ray evidence for the lack of a long-period dependence on annealing time.[5] The thickening of the crystallites is the major contribution to the increase in long period. From Tables V and VI it is clear that the noncrystalline regions either remain roughly constant or increase slightly in size. No indication of shrinkage of noncrystalline domains is present from the modeling of diffusion rates. This suggests that annealing causes substantial rearrangement of domains and that a one-dimensional lamellar model cannot be strictly correct since the expansion of the crystallites does not apparently reduce the average noncrystalline domain sizes, although it does result in an overall drop in the fraction of noncrystalline material.

The crystallite size determined by NMR and presented in Tables V and VI indicates the distance across the thinnest dimension of the crystallite. This distance ranges from roughly 3 nm in the control sample to 7 nm in the samples annealed above 200 °C. If the chains are assumed to be collinear with the direction corresponding to the thinnest dimension of the crystallites (as is reasonable from the agreement between the NMR long period and the SAXS axial long period), the corresponding numbers of monomer repeat units which can be incorporated into such crystallites before the chains emerge into noncrystalline regions are 3 and 7, respectively. This behavior helps to explain the increase in the long T_{1xz} as a function of annealing, as is shown by data in Table II. We suggest that for the control sample the crystallites are sufficiently thin that the chain segments in the interior of the crystallites can feel effects of the nearby noncrystalline mobility. These crystalline chains display more mobility than their counterparts in the annealed samples, which are included in crystals more than twice as thick. The long T_{1xz}'s reflect the mobility difference, increasing from 71 ms in the control sample to 280 ms in sample N. Apparently, it is the relatively small size of the PET crystals which allows such motional differences to be exhibited.

The use of spin diffusion to obtain relative surface areas of crystallites is an important aspect of these experiments. Such information is not available from commonly used techniques. The data in Table IX indicate that annealing above 200 °C is most effective in reducing the surface area/volume ratio for PET crystals; roughly a 30% reduction in surface areas is obtained. The moderate size of this reduction as well as the agreement of the data with surface areas calculated from the one-dimensional lamellar models suggests that the shape of the crystallites is not highly irregular. (In fact, if highly accurate surface area/volume ratios were obtained for a wide range of annealing temperatures, it should be possible to extract details of the crystallite shape.) Again we emphasize that the attractive feature of determining surface areas in this way is that the analysis at short times does not rely on a morphological model.

In each of the NMR experiments presented above, samples D200-22 and D200-0 behave similarly. Their crystallinities, relative surface areas, and domain sizes are in close agreement with one another. Such evidence suggests that annealing either with or without free ends has little effect on the domain structure of PET fibers. However, D200-22, annealed with free ends, has a substantially lower modulus (60% lower) and much poorer creep resistance (6 times more elongation) than does D200-0. This deterioration in certain mechanical properties appears to be related primarily to a loss in orientation of both crystalline and noncrystalline chains. This loss can be followed most effectively by ^{13}C NMR and X-ray fiber diffraction.

Finally, we comment on the structure of PET prior to annealing. As-drawn fibers such as the control sample do have small crystalline regions, as indicated by the presence of a long T_{1xz} component. Small-angle X-ray evidence has been used in the past to suggest that such samples are almost entirely noncrystalline.[57] The small size of the crystallites (~3 nm in the thinnest dimension) may cause difficulty with respect to X-ray detection and quantitation. The SAXS measurements of our sample C, on the other hand, did not encounter such problems and allowed definition of both the axial long period and a transverse periodicity from the four-point pattern. The question of organized structure in PET film quenched from the melt (sample Q) is more complicated. Three T_{1xz}'s are resolved in the decay under multiple pulse, with the longest being 26 ms. This result certainly indicates some degree of motional heterogeneity throughout the sample but does not suggest the degree to which structural heterogeneity is involved. Such structural information is available from the spin diffusion experiment, which defines the size of the regions over which the motion is reasonably homogeneous. In the semicrystalline samples the noncrystalline material is segregated into two domains whose average smallest dimension is on the order of a few nanometers. However, in sample Q the spin diffusion experiment does not allow the definition of discrete domains of finite size. The decompositions of the T_{1xz} decays for various diffusion times reveal fractions of the three components which do not behave systematically in terms of magnetization recovery into initially depleted regions. From this information we conclude that the mobile and constrained noncrystalline chain segments are segregated into discrete domains in semicrystalline PET to a much greater degree than they are in the pure glass. The coarseness of structural heterogeneity in the noncrystalline material of the

fibers and annealed film appears considerably greater.

Summary and Conclusions

Based upon the foregoing NMR data, we offer the following conclusions concerning the morphology of PET fibers.

Annealing PET above its T_g increases crystallinity, with temperatures greater than 200 °C being most effective. Annealing also increases the minimum crystallite dimension and the long period as determined by NMR. We suggest that the NMR methods discussed above may quantify these changes more satisfactorily than do other techniques. We also emphasize that NMR can give direct information on both crystalline and noncrystalline domains, in contrast to X-ray scattering. From the increase in the long time constants measured under multiple pulse, it is clear that annealing increases the rigidity of chains in the crystallites. This points toward a correlation between crystallite size and chain mobility for semicrystalline PET.

A two-phase, crystalline/amorphous model is seen to be a poor representation of PET fiber morphology. The noncrystalline material can be divided into mobile and constrained parts, each of which has some direct contact with crystallites. A picture in which there is a uniform gradation from rigid to semirigid to mobile material is not entirely accurate. Upon annealing, the crystallites grow by absorbing both types of noncrystalline chains. On the basis of the spin diffusion results, structural heterogeneity in the noncrystalline material of the fibers is considerably coarser than it is in the quenched, amorphous film.

Whether annealing of PET fibers at 200 °C is done with free ends or with fixed ends makes little difference with respect to crystallinity, domain size, and crystallite surface areas, although there is a trend in the T_{1xz} data which suggests that the chains in all regions of the fibers annealed with free ends experience slightly greater constraint than do their counterparts in the fibers annealed with fixed ends. Chain orientation in fibers annealed without restraint deteriorates strongly, which largely explains the reduced modulus and creep resistance observed in mechanical testing.

Finally, reliable measurements of crystallite surface areas are possible by recording initial spin diffusion rates. Annealing PET above 200 °C reduces the surface area/volume ratio by ~30%, whereas annealing at 200 °C has a considerably smaller effect. Such information concerning domain surface areas is thought to be an important aspect of many polymer systems, although experimental data have proved difficult to obtain. This is one area in which the NMR methods discussed here should find expanded use.

Acknowledgment. We thank V. Mochel and G. Böhm of Firestone for providing the samples and for collaborating in this work from the beginning. We thank K. W. Zilm for his contributions to the measurement of $T_{1\rho}$ values and for stimulating discussions during his brief stay at NBS. We are also grateful to R. Boisvert for his help with the computing and to A. J. Vega, C. Guttman, E. DiMarzio, and C. Han for useful discussions. J.R.H. thanks the National Research Council for a postdoctoral fellowship.

References and Notes

(1) R. de P. Daubeny, C. W. Bunn, and C. J. Brown, *Proc. R. Soc. London, Ser. A*, **226**, 531 (1954).
(2) J. H. Dumbleton, *Polymer*, **10**, 539 (1969).
(3) D. E. Bosley, *J. Appl. Polym. Sci.*, **8**, 1521 (1964).
(4) S. Fakirov, E. W. Fischer, and G. F. Schmidt, *Makromol. Chem.*, **176**, 2459 (1975).
(5) E. W. Fischer and S. Fakirov, *J. Mater. Sci.*, 11, 1041 (1976).
(6) R. J. Matyi and B. Crist, *J. Macromol. Sci., Phys.*, **B16**, 15 (1979).
(7) W. Wu, H. G. Zachmann, and C. Rickel, *Polym. Commun.*, **25**, 76 (1984).
(8) S. Fakirov, E. W. Fischer, R. Hoffman, and G. F. Schmidt, *Polymer*, **18**, 1121 (1977).
(9) E. H. Müller, *Colloid Polym. Sci.*, **252**, 696 (1974).
(10) W. J. Dulmage and A. L. Geddes, *J. Polym. Sci.*, **31**, 499 (1958).
(11) J. L. Koenig and S. W. Cornell, *J. Polym. Sci., Part C*, **22**, 1019 (1969).
(12) W. O. Statton, J. L. Koenig, and M. Hannon, *J. Appl. Phys.*, **41**, 4290 (1970).
(13) A. Cunnigham, I. M. Ward, H. A. Willis, and V. Zichy, *Polymer*, **15**, 749 (1974).
(14) B. Jasse and J. L. Koenig, *J. Macromol. Sci., Rev. Macromol. Chem.*, **C17**, 61 (1979).
(15) A. Garton, D. J. Carlsson, and D. M. Wiels, *Text. Res. J.*, **51**, 28 (1981).
(16) M. Kashiwagi, A. Cunningham, A. J. Manuel, and I. M. Ward, *Polymer*, **14**, 111 (1973).
(17) A. Cunningham, A. J. Manuel, and I. M. Ward, *Polymer*, **17**, 126 (1976).
(18) H. G. Zachmann, *Polym. Eng. Sci.*, **19**, 966 (1979).
(19) M. D. Sefcik, J. Schaefer, E. O. Stejskal, and R. A. McKay, *Macromolecules*, **13**, 1132 (1980).
(20) K. R. Lucas, V. D. Mochel, L. I. Slutsker, and G. G. A. Böhm, to be published.
(21) N. Bloembergen, *Physica (Utrecht)*, **15**, 386 (1949).
(22) M. Goldman and L. Shen, *Phys. Rev.*, **144**, 321 (1966).
(23) T. T. P. Cheung and B. C. Gerstein, *J. Appl. Phys.*, **52**, 5517 (1981).
(24) T. T. P. Cheung, *J. Chem. Phys.*, **76**, 1248 (1982).
(25) R. A. Assink, *Macromolecules*, 11, 1233 (1978).
(26) T. T. P. Cheung, B. C. Gerstein, L. M. Ryan, R. E. Taylor, and C. R. Dybowski, *J. Chem. Phys.*, **73**, 6059 (1980).
(27) C. R. Dybowski and R. G. Pembleton, *J. Chem. Phys.*, **70**, 1962 (1979).
(28) K. J. Packer, J. M. Pope, R. R. Yeung, and M. E. A. Cudby, *J. Polym. Sci., Polym. Phys. Ed.*, **22**, 589 (1984).
(29) A. Abragam, "Principles of Nuclear Magnetism", Oxford University Press, London, 1961.
(30) U. Haeberlen, "High Resolution NMR in Solids", Academic Press, New York, 1976.
(31) M. Mehring, "Principles of High Resolution NMR in Solids", Springer-Verlag, New York, 1983.
(32) A. J. Vega and R. W. Vaughan, *J. Chem. Phys.*, **68**, 1958 (1978).
(33) A. J. Vega, A. D. English, and W. Mahler, *J. Magn. Reson.*, **37**, 107 (1980).
(34) M. D. Sefcik, J. Shaefer, E. O. Stejskal, and R. A. McKay, *Macromolecules*, **13**, 1132 (1980).
(35) A. D. English, *Macromolecules*, **17**, 2182 (1984).
(36) B. C. Gerstein, *Phil. Trans. R. Soc. London, Ser. A*, **299**, 521 (1981).
(37) J. R. Havens and D. L. VanderHart, *J. Magn. Reson.*, **61**, 389 (1985).
(38) P. Mansfield, M. J. Orchard, D. C. Stalker, and K. H. B. Richards, *Phys. Rev.*, **B7**, 90 (1973).
(39) W.-K. Rhim, D. D. Elleman, and R. W. Vaughan, *J. Chem. Phys.*, **59**, 3740 (1973).
(40) W.-K. Rhim, D. D. Elleman, L. B. Schreiber, and R. W. Vaughan, *J. Chem. Phys.*, **60**, 4595 (1974).
(41) Certain commercial materials and instruments are identified in this paper to specify adequately the experimental procedure. In no instance does such identification imply recommendation or endorsement by the National Bureau of Standards nor does it imply that the material or instrument is necessarily the best available for the purpose.
(42) J. D. Ellett, M. G. Gibby, U. Haeberlen, L. M. Huber, M. Mehring, A. Pines, and J. S. Waugh, *Adv. Magn. Reson.* **5**, 117 (1971).
(43) R. W. Vaughan, D. D. Elleman, L. M. Stacey, W.-K. Rhim, and J. W. Lee, *Rev. Sci. Instr.*, **43**, 1356 (1972).
(44) D. J. Adduci, P. A. Hornung, and D. R. Torgeson, *Rev. Sci. Instrum.*, **47**, 1503 (1976).
(45) A. N. Garroway, P. Mansfield, and D. C. Stalker, *Phys. Rev. B*, **11**, 121 (1975).
(46) S. Idziak and U. Haeberlen, *J. Magn. Reson.*, **50**, 281 (1982).
(47) D. Horne, R. D. Kendrick, and C. S. Yannoni, *J. Magn. Reson.*, **52**, 299 (1983).
(48) D. P. Burum, M. Linder, and R. R. Ernst, *J. Magn. Reson.*, **43**, 463 (1981).
(49) H. Post and U. Haeberlen, *J. Magn. Reson.*, **40**, 17 (1980).

(50) R. Freeman, T. A. Frenkiel, and M. H. Levitt, *J. Magn. Reson.*, **44**, 409 (1981).
(51) M. Lee and W. I. Goldburg, *Phys. Rev.*, **140**, A1261 (1965).
(52) H. S. Carslaw and J. C. Jaeger, "Conduction of Heat in Solids", Oxford University Press, Oxford, 1947.
(53) J. Crank, "The Mathematics of Diffusion", Oxford University Press, Oxford, 1956.
(54) G. K. Leaf, M. Minkoff, G. D. Byrne, D. Sorensen, T. Bleakney, and J. Saltzman, DISPL, ANL-77-12 Rev 1, National Technical Information Service, Springfield, VA, 1978.
(55) G. Farrow and I. M. Ward, *Polymer*, **1**, 330 (1960).
(56) D. E. Bosky, *J. Polym. Sci., Part C*, **20**, 77 (1967).
(57) J. H. Dumbleton, *J. Polym. Sci. Part A-2*, **7**, 667 (1969).
(58) D. C. Douglass and G. P. Jones, *J. Chem. Phys.*, **45**, 956 (1966).

Hydrogen Bonding in Polymers: Infrared Temperature Studies of an Amorphous Polyamide

Daniel J. Skrovanek, Stephen E. Howe, Paul C. Painter, and Michael M. Coleman*

Polymer Science Program, Department of Materials Science, The Pennsylvania State University, University Park, Pennsylvania 16802. *Received December 21, 1984*

ABSTRACT: Fourier transform infrared temperature studies of an amorphous polyamide are presented. The results strongly suggest that prior interpretations of the changes occurring in the N–H stretching region of the spectra of polyamides and polyurethanes with temperature were greatly oversimplified. In essence, these spectral changes were interpreted to be solely due to hydrogen-bonded N–H groups transforming to "free" N–H groups. Subsequent use of these data to obtain thermodynamic parameters associated with hydrogen bond dissociation must now be considered erroneous. The primary factor not taken into account concerns the very strong dependence of the absorption coefficient with hydrogen bond strength. With increasing temperature, the average strength of the hydrogen bonds decreases, which is observed in the infrared spectrum by a shift to higher frequency. Concurrently, the absorption coefficient decreases, leading to a reduction in the absolute intensity of the hydrogen-bonded N–H band. In this study we present experimental results in the N–H stretching and amide I, II, and V regions of the infrared spectrum of an amorphous polyamide. In addition, we present a model, justified by theoretical considerations, which we believe advances our understanding of the strong dependence of absorption coefficient with the strength of the hydrogen bonds. The ramifications of this work to hydrogen-bonded polymers are discussed.

Introduction

Over the past several years, we have been concerned with the application of Fourier transform infrared (FT-IR) spectroscopy to the characterization of polymer mixtures. Information concerning the nature, strength, and number of intermolecular interactions occurring between the polymeric components of such mixtures as a function of temperature has been gained. The thrust of this work, summarized in a recent review,[1] has been to relate these measurements to the phase behavior of polymer blends. Patterson and Robard[2] consider the phase behavior to be governed by two competing factors: a free volume contribution to the equation of state which is unfavorable to mixing and an interactional contribution which is potentially favorable to mixing. In our studies we have placed emphasis on the "interactional" component and it is intuitively clear that there has to be a corresponding balance between strength of intermolecular interactions among the different components of the blend and the forces of self-association. Because of these factors, we have paid particular attention to systems in which strong intermolecular interactions occur, characteristically those involving hydrogen bonds. This has led us to consider the infrared methods that have previously been used to determine thermodynamic parameters. For example, in a recent publication,[3] we presented the results of an FT-IR temperature study of poly(4-vinylphenol) blends containing poly(vinyl acetate) and three ethylene–vinyl acetate copolymers. From a quantitative measure of the fraction of hydrogen-bonded carbonyl groups as a function of temperature, we obtained an estimation of the enthalpy of the intermolecular interaction from a van't Hoff plot. There were many assumptions inherent in this calculation, but the estimated value of ΔH was in pleasing agreement with previously published values for low molecular weight analogues. This result is probably fortuitous because we now believe that there are major problems associated with methods previously used to determine such parameters from spectroscopic data.

Extensive research on hydrogen bonding in polyamides and polyurethanes has been performed by numerous authors.[4-14] Trifan and Terenzi[4] concluded that at room temperature there is essentially 100% hydrogen bonding in linear, aliphatic homopolyamides, as measured by the absence of bands in the infrared spectra above 3300 cm^{-1}. However, in structurally irregular copolymers and in linear homopolyamides at elevated temperatures, an absorption at 3448 cm^{-1} was observed and assigned to "free" N–H groups. Bessler and Bier[6] measured the "free" and bonded N–H peak heights of various polyamides as they change with temperature. Analysis was complicated, however, by the overlap and inherent broadeness of the infrared bands, especially at elevated temperatures.

A quantitative study of hydrogen bond dissociation in polyamides was performed by Schroeder and Cooper.[13] In an elegant procedure which avoids curve resolving, these authors reasoned that if one has a knowledge of the absorption coefficients corresponding to the "free" and bonded N–H stretching modes, then it is only necessary to measure the total area of the N–H stretching region to obtain the required data. In other words, when the temperature is raised, the change in total area reflects the difference in absorption coefficients as the bonded N–H groups transform to "free" N–H groups. Two assumptions were necessary: that the absorption coefficients did not vary significantly with temperature and that the degree of hydrogen bonding was known at some reference temperature. The data obtained were used, via an equilibrium

0024-9297/85/2218-1676$01.50/0